Electrochemical Performance and Preliminary Post-Mortem Analysis of a Solid Oxide Cell Stack with 20,000 h of Operation

Qingping Fang,[z] Carolin E. Frey, Norbert H. Menzler,[*] and Ludger Blum

Institute of Energy and Climate Research (IEK), Forschungszentrum Jülich GmbH, 52425 Jülich, Germany

A long-term test with a two-layer solid oxide cell stack was carried out for more than 20,000 hours. The stack was mainly characterized in a furnace environment in electrolysis mode, with 50% humidification of H_2 at 800°C. The endothermic operation was carried out with a current density of −0.5 Acm^{-2} and steam conversion rate of 50%. Electrolysis at lower temperatures (i.e., 700°C and 750°C) and fuel cell operation (with 0.5 Acm^{-2} and fuel utilization of 50%) at 800°C were also carried out (<2000 h each) for comparison. The voltage and area specific resistance degradation rates were ∼0.6%/kh and 8.2%/kh after ∼18,460 hours of operation. In total, the stack was operated above 700°C for more than 20,000 hours. Impedance measurement and analysis showed that the increase of ohmic resistance was the main degradation phenomenon, while electrode polarizations were kept nearly constant before a severe burning took place in one layer. Ni-depletion in fuel electrodes was confirmed during post-mortem analysis, which was assumed to be the major degradation mechanism observed. The stack performance and degradation analysis under different working conditions, as well as the results of preliminary post-mortem analysis will be presented.

 [DOI: 10.1149/2.0541802jes]

Manuscript submitted November 10, 2017; revised manuscript received December 27, 2017. Published January 9, 2018.

One of the critical challenges to the application and commercialization of solid oxide cell (SOC) technology is the long-term stability of complete systems, stacks and single components. Despite the fact that accelerating methods have long been under discussion, the time-consuming and costly endurance tests of stacks and cells under relevant conditions are still necessary for reliable degradation analyses and lifetime prediction. Compared to the tests with single cell or other stack and system component, the results of long-term degradation tests with stacks are quite limited.[1–5] Previous results have shown stable performance of stacks working in the temperature range of 700–800°C in SOFC mode.[6–9] Recently, a short stack achieved a 10 years lifetime, and remains in operation.[10] With proper protective coating, a voltage degradation rate of less than 0.3%/kh and lifetime of more than 40,000 h at 700°C is possible with current stack design and components. In contrast to the low degradation rate in SOFC mode, higher degradation rates of ∼0.6–1.5%/kh were observed with similar types of cells in the same stack design in SOEC mode, as described by Nguyen et al.[11] Therefore, the functionality and optimization potential of the cells and stacks, as well as their long-term degradation behavior and mechanisms in SOEC mode, needs to be further investigated. Amongst the stacks operated in SOEC mode, a two-layer stack was operated under different stationary conditions for more than 20,000 h. The stack performance was regularly monitored by open circuit voltage, voltage-current curves and impedance measurements. After cooling down, one third of the stack was embedded in resin for cross-section preparation, and the rest was disassembled for visual inspection. The preliminary results of the post-mortem analysis will be also presented.

Experimental

The performance of the stack (stack number: F1002-165) up to the first 5000 h of operation was previously presented by Fang et al.[12] The detailed descriptions of the stack and experimental setup, including temperature measurement and steam generation, etc. can be found there. The cells used were ASCs (anode-supported cells in fuel cell mode) with an active area of 80 cm^2 produced in-house with 8YSZ (8 mol-% yttria-stabilized zirconia) thin electrolytes (∼10 μm) and LSCF air electrodes ($La_{0.58}Sr_{0.4}Co_{0.2}Fe_{0.8}O_{3-\delta}$).

After standard joining, conditioning and characterization procedures as described in Ref. 12, the stack was first operated with a current density of −0.5 Acm^{-2} and steam conversion rate of 50% at the furnace temperatures of 800°C, 750°C and 700°C, respectively. Then, a period of fuel cell operation with a current density of 0.5 Acm^{-2} and fuel utilization rate of 50% was carried out at 800°C before initiating the long-term electrolysis.

During stationary operation, electrical load was interrupted regularly and impedance measurements were performed under open circuit voltage (OCV) condition. The current EIS setup includes an FC350 fuel cell monitor (Gamry), an electronic load ZS4812 (H&H) and N5763A power supply (Agilent Technologies). The frequency range was from 0.1 Hz to 10 kHz, with 10 points per decade, and an AC current of 2 A. To avoid switching between fuel cell and electrolysis modes during impedance measurements with the AC current, a small DC offset of ±5 A (i.e. ±0.0625 Acm^{-2}) was applied during the measurements (+5 A for fuel cell mode, −5 A for electrolysis mode). All parameters were chosen on the basis of previous experiments. The distribution function of relaxation times (DRT)[13–15] was calculated from the real part of the measured impedance data by employing the FTIKREG[16] software package from the CPC Program Library.

Results and Discussion

The complete time plot of stack F1002-165 is shown in Figure 1. The standard liter per minute (slm) is used for flow rate in this work.

The calculated area-specific resistances (ASRs) of the cells are also shown in Figure 1. The ASR was calculated from the difference between the average Nernst voltage and the measured voltage at the given current density. The average Nernst voltage is calculated according to the gas compositions at the inlet and outlet of the stack. Note, the gas composition at the outlet was not measured, but only calculated based on the inlet composition and fuel utilization or steam conversion rate. No effect of leakages inside the stack was considered. Therefore, the calculated ASRs would be smaller than the real ones in electrolysis mode, when the leakages are no longer negligible (e.g., periods VIII and IX in Figure 1).

The different operational periods of the stack are marked in Figure 1 with roman numerals. Detailed testing conditions are shown in Table I. During stationary operation, the gas composition of 50% H_2 and 50% H_2O was kept constant. The steam conversion rate (i.e., fuel utilization in fuel cell mode) and current density were kept at 50% and −0.5 Acm^{-2} (0.5 Acm^{-2} in fuel cell mode), respectively. The calculated average degradation rates for each period are also shown in Table I.

The stack performance, degradation and gas tightness were monitored through voltage –current (U-j) curves, impedance measurements and OCVs. A comparison of the U-j curves at the end of operation periods I, VII, VIII and IX is shown in Figure 2. Both layers showed

*Electrochemical Society Member.
[z]E-mail: q.fang@fz-juelich.de

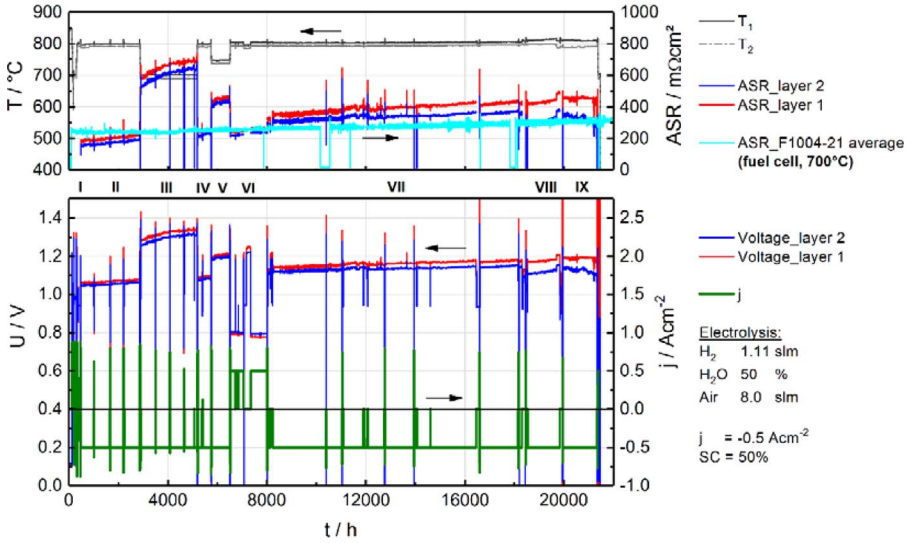

Figure 1. Time plot of stack F1002-165.

Table I. Operating information of the stack (H_2:H_2O = 1:1 for stationary operation).

Period	Duration (h)	Stack Temperature (°C)	Current density (Acm^{-2})	Fuel/steam utilization	Voltage degradation (/kh)	ASR degradation (/kh)
I	450	600∼800°C		≤80%	n.a.	n.a.
II	2400	800°C	-0.5	50%	0.7%	10.1%
III	2300	700°C	-0.5	50%	1.9%	9.0%
IV	500	800°C	-0.5	50%	0.8%	9.1%
V	700	750°C	-0.5	50%	1.9%	11.3%
VI	1500	800°C	0.5	50%	<0.1%	0.6%
VII	10000	800°C	-0.5	50%	0.4%	2.7%
VIII	1300	800°C	-0.5	50%	1.0%	8.5%
IX	1300	800°C	-0.5	50%	<0	n.a.

similar performance in either fuel cell or electrolysis mode at the beginning of the operation. After 18,460 h of operation (end of period VII) a decrease in OCV could be observed in layer 2. The resistance of layer 2 in electrolysis mode was also clearly lower than that of layer 1, which could be due to the locally-decreased steam conversion rate in layer 2 as a result of the leakage. During the last 2600 h of operation (periods VIII, IX), the leakage in layer 2 increased significantly. The voltage degradation rates in the testing period of 500 h∼18,460 h of operation calculated at ±0.5 Acm^{-2} are 0.6–0.7%/kh, which agrees well with the values determined from the voltage-time plot.

The increased leakage inside the stack could also be confirmed by the OCVs with dry hydrogen as shown in Figure 3. The OCV of layer 2 decreased from 1.2 V to 1.18 V after ∼5000 h of operation (periods I-III), while the OCV of layer 1 did not degrade at all. Until ∼8000 h of operation (end of period VI), OCVs of both cells were fairly

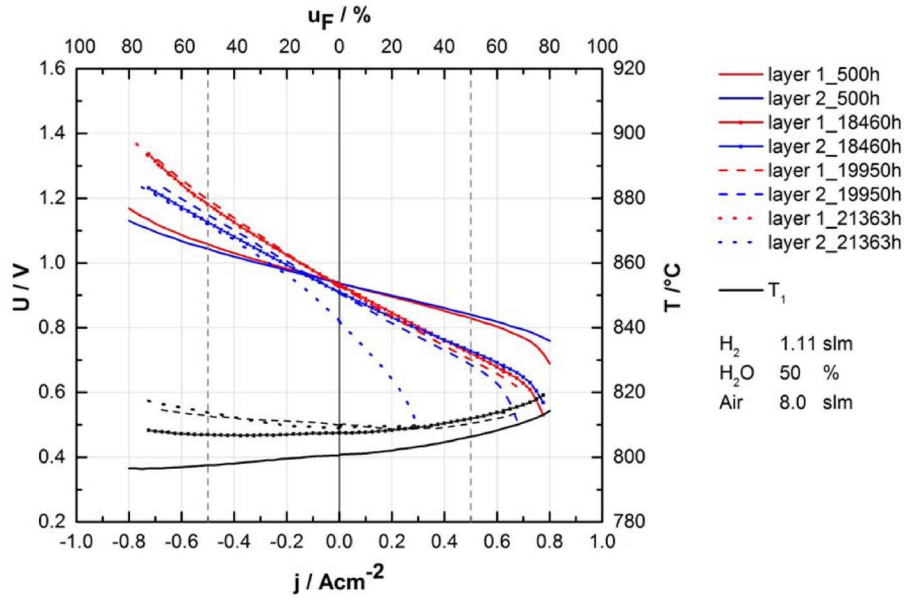

Figure 2. Comparison of the U-j curves measured before stationary operation (end of period I, 500 h), end of period VII (18,460 h), end of VIII (19,950 h) and end of period IX (21,363 h).

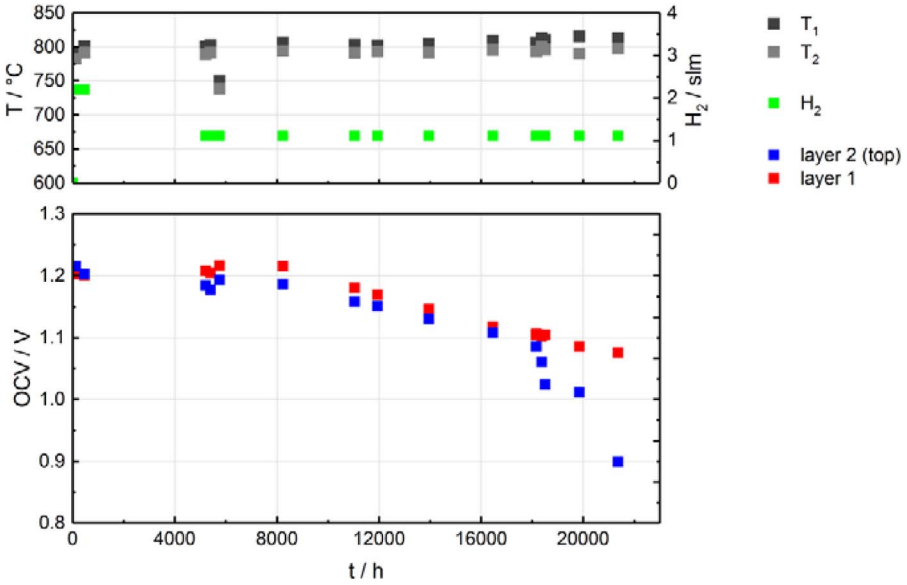

Figure 3. OCVs of both layers with dry hydrogen.

stable. Thereafter, they decreased simultaneously and continuously to about 1.1 V during ∼10,000 h of electrolysis at 800°C (period VII). Although 1.1 V was still a satisfactory voltage (representing a good gas tightness of both layers), it indicated that the leakage was increasing during the operation. The reason of the leakage will be discussed together with the results of post mortem analysis. The stack suffered several unplanned load cycles at ∼18,000 h due to failures of different components in the test bench (i.e., evaporator, pump, heating band, computer, etc.). The leakage rate had then increased dramatically in layer 2. At the end of the test, layer 2 showed an OCV of only 900 mV compared to 1076 mV of layer 1, with a total H_2 flow rate of 1.11 slm at the stack inlet. According to the Nernst equation, those voltages correspond to a water content of 70% in layer 2 and 5% in layer 1, supplying dry H_2 at 800°C. Assuming a uniform gas distribution to the two layers, there must be a certain amount of H_2 consumed if the low OCV in layer 2 was due to a short circuit or a large leakage. However, the H_2 flux at the stack outlet measured with a mass flowmeter after condensation was still 0.94 slm, which cannot explain the low OCV of layer 2 based on a short circuit (must be lower). Therefore, the previous assumption of a homogeneous fuel flow distribution can no longer hold. Assuming the low OCV was due to a leakage, the amount of H_2 passing through each layer can be calculated based on the Nernst equation and the measured H_2 flow rate. With the inlet flow rate of 1.11 slm and outlet flow rate of 0.94 slm, the amounts of H_2 through layer 1 and layer 2 were calculated to be 0.93 slm and 0.18 slm, respectively. As can be seen from the last U-j curve in Figure 2, layer 2 started to show a concentration polarization at 0.25 Acm^{-2}, which corresponded to a nominal fuel utilization of 30%. With a "real" H_2 flow of 0.18 slm, the fuel utilization will be ∼80% at 0.25 Acm^{-2}, which explains the diffusion polarization behavior.

On the basis of the above analysis, the following results can be concluded:

- The voltage degradation rate during electrolysis at 800°C was 0.7%/kh for the first 2400 h of operation (period I). Operation at lower temperatures (periods III and V) did not significantly influence the degradation behavior at 800°C (periods IV and VII). The degradation rate was decreasing during the 10,000 h of operation (period VII), which was mostly due to the decreasing steam conversion rate as a result of the increasing leakage inside the stack.
- The voltage degradation rates during electrolysis at 700°C and 750°C (periods III and V) were higher than that at 800°C, especially at the beginning of each operation. However, the average ASR degradation rates at all three temperatures are comparable with the operation time.
- After about 6000 h of operation in electrolysis mode, the stack showed almost no degradation during stationary operation in fuel cell mode (period VI). However, voltage losses could be noticed from time to time after load cycles during the entire operation.
- The possible recovery of the stack performance by reversible operation during electrolysis is difficult to evaluate due to the relatively short operation time in fuel cell mode, which requires further investigation.
- The cell voltage of layer 2 was much lower than the other one during the last two operation periods (VIII and IV). At the end of period VIII, the furnace temperature had to be decreased by ∼10°C to avoid overheating of the stack. Both (voltage and temperature) indicated that layer 2 in particular had a large degree of leakage, which explains the negative degradation during electrolysis observed in period IX.
- The total average degradation rates of the stack up to period VII, including all losses during load cycles, were 0.6%/kh and 8.2%/kh, respectively, for voltage and ASR degradation.
- As a reference, the ASR evolution of an SOFC stack (stack number: F1004-21) equipped with the same type of cells, which was operated at 700°C for ∼35,000 h with a low voltage degradation rate of 0.3%/kh and ASR degradation rate of 1.0%/kh, is also presented in Figure 1. Under current testing conditions, the stack/cells degraded faster in electrolysis mode than in fuel cell mode, indicating/confirming different degradation mechanisms.

The impedance spectra of both layers in SOFC and SOEC modes, taken under the OCV condition, are shown in Figure 4. Without the last measurement, there seems to be mainly a shift of the spectrum to the right in the Nyquist plot for both layers, indicating a continuous increase of the ohmic resistance throughout the entire operation. Additionally, a progressive enlargement of the high frequency arc can be noticed. During the last measurement, a large diffusion process was added in layer 2, which corresponded to the aggressive degradation after the last period of operation. The intersections of the spectra with the real-axis were used to analyze the evolution of ohmic resistance, polarization and total resistance, as shown in Figure 5. The ohmic resistance and polarization were of similar magnitude while starting the test. Although slight increases in polarization could be observed, especially with layer 2, during the last ∼5000 h of operation, the faster growing ohmic resistance dominated the entire degradation process. After ∼20,000 h, the ohmic resistances of both layers were more than triple the starting values. Possible explanations of the continuous increase in the ohmic resistance include grain growth in the electrolyte, pore formation near the 8YSZ/GDC (gadolinium doped ceria)

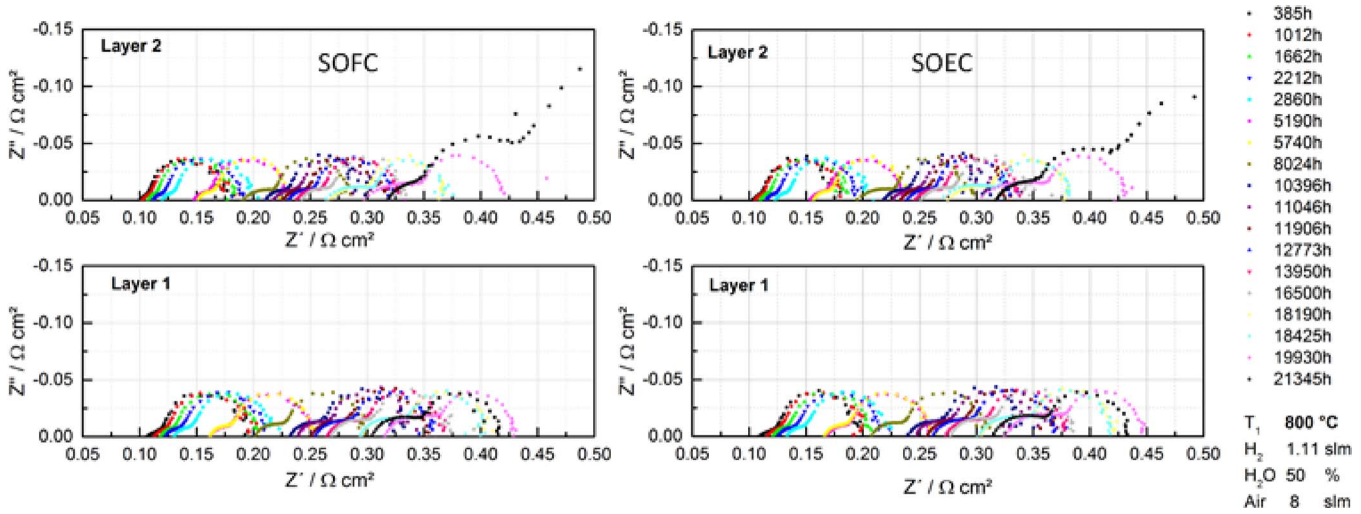

Figure 4. Impedance spectra of both layers at 800°C in SOFC (left) and SOEC (right) modes.

interface, as reported by Schefold et al.[17] and Tietz et al.,[18] and depletion of nickel near the boundary of the electrolyte and fuel electrode as observed by different groups.[19–22] The effective ionic conductivity of the composite electrodes is usually below 10% of that of the bulk electrolyte depending on the porosity and volume fraction of the composites according to Zheng et al.[23] Therefore, the increase of ohmic resistance can be one of the consequences of Ni depletion in Ni/YSZ electrode, which shifts the working electrode area outwards and increases the electrolyte thickness. Note that the polarization and total resistance of layer 2 from the last measurement are not presented in Figure 5.

The distribution of relaxation times of layer 1 and layer 2 in both SOFC and SOEC modes are shown in Figure 6 and Figure 7, respectively. According to the previous results in Fang et al.,[12] the peaks in the frequency ranges of 1–10 Hz and 10–300 Hz correspond to the gas diffusion in the substrate and to the chemical surface exchange of O_2 and O^{2-} bulk diffusion in the air electrode. Obviously, there was a slight decrease in gas diffusion polarization and an increase in air electrode polarization in both layers. Starting from 18,190 h, an increasing of the third peak at ∼1000 Hz became obvious, which indicates increasing degradation in the fuel electrode of layer 2. The impedance spectrum of the last measurement of layer 2 was so different from the rest of the measurements that a different regularization factor (i.e., $\lambda = 200$ instead of 1000, if not stated otherwise in this work) in the DRT analysis had to be used. As shown in Figure 7, a large half peak at 0.1 Hz, which corresponds to O_2 diffusion in the air electrode, was observed in layer 2 at the end of the operation. In normal cases, such a peak at low frequency is only visible when the oxygen partial pressure at the air electrode is lower than 5%, as mentioned in Leonide[24] and Fang et al.[12] The reason for the increased diffusion polarization in the air electrode was examined in the post-mortem analysis.

After cooling down, one third of the stack was embedded in resin for cross-section preparation, while the rest was disassembled for visual inspection. Figure 8 shows both air and fuel sides of the two layers. During the disassembly, the following effects could be observed:

- Both cells cracked during the disassembly, but should have been intact during stack operation. Otherwise, any trace of burning would have been observed in the active cell region on either the anode or cathode side.
- Fuel electrode substrates of both cells were intact.
- Delamination of the air electrode (5∼10% of the total cell area, partially with the electrolyte) took place in both layers on the air inlet side (i.e. the fuel outlet side). With the stack configuration of the counter flow, the local current density at the air inlet is smaller than that on the outlet side in electrolysis mode. Why the delamination occurred at the region of lower current density is not yet understood.
- Strong burning could be seen in layer 2 on the air outlet side (i.e. the fuel inlet side) in the manifold region. As a consequence, a certain amount of hydrogen in layer 2 was combusted at the front

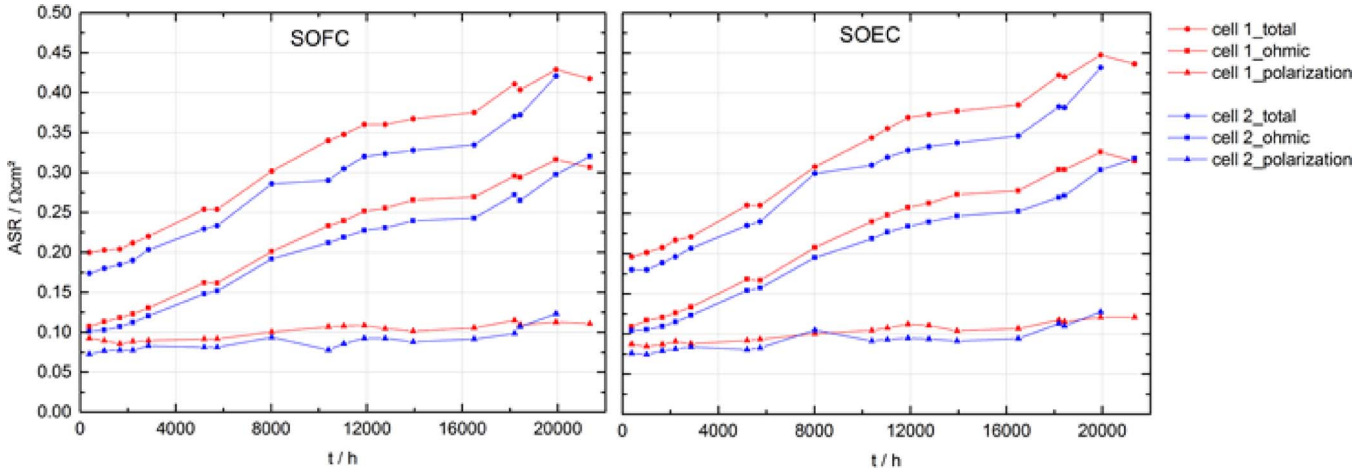

Figure 5. Evolution of the ohmic resistance, polarization and total resistance of both layers.

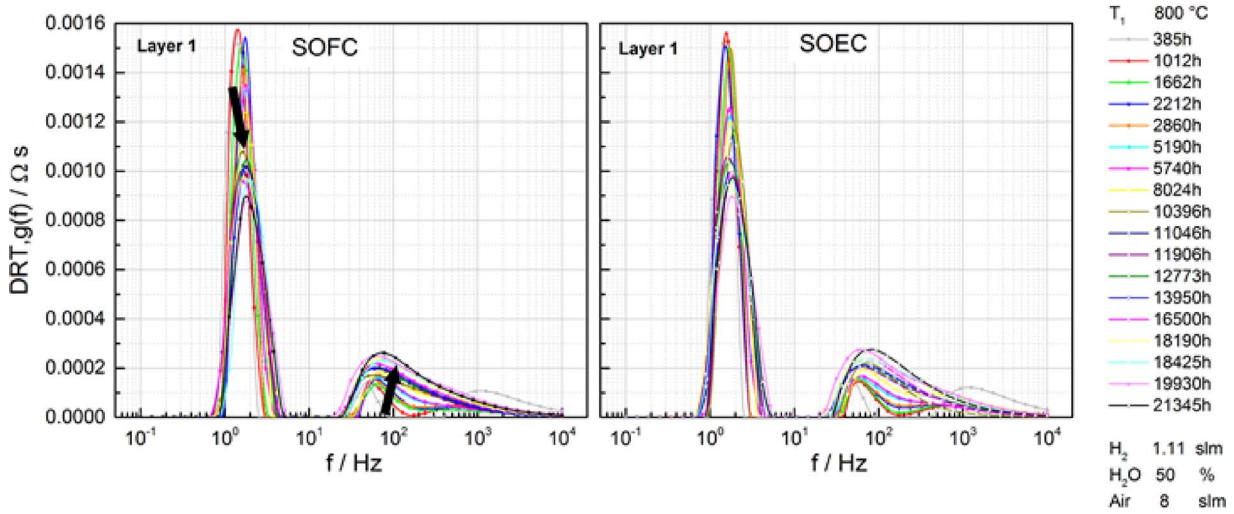

Figure 6. The DRT curves of layer 1 at 800°C in SOFC (left) and SOEC (right) modes, calculated using the real part of the impedance spectra.

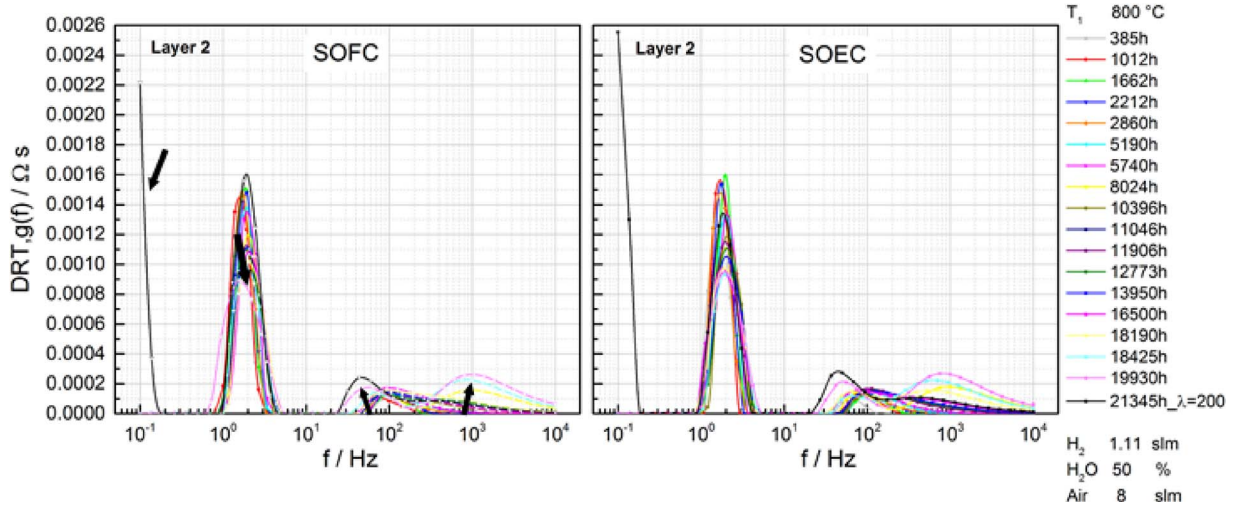

Figure 7. The DRT curves of layer 2 at 800°C in SOFC (left) and SOEC (right) modes, calculated using the real part of the impedance spectra.

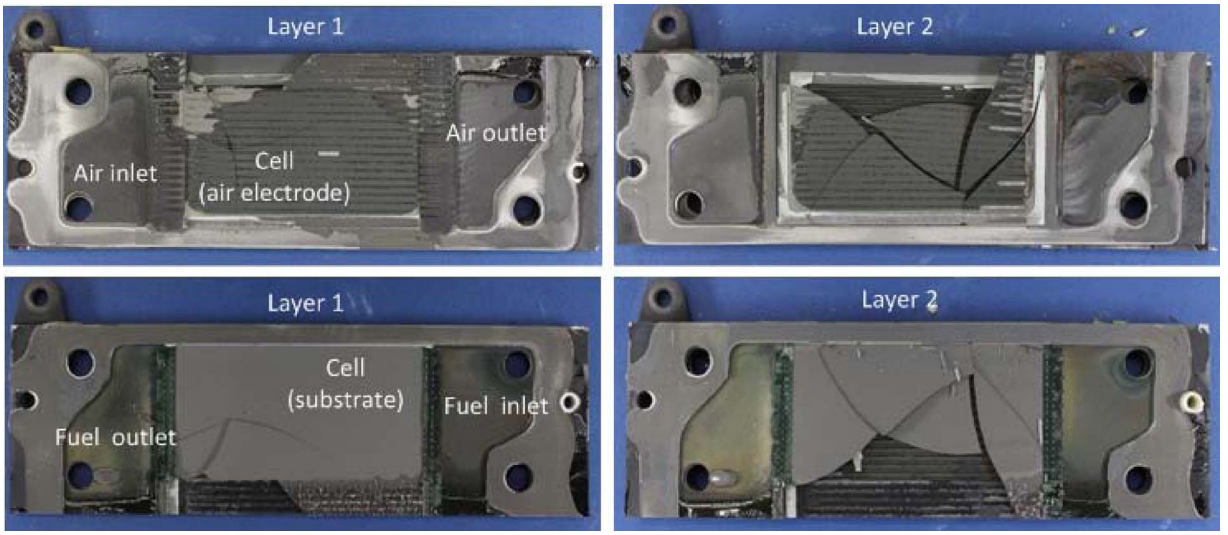

Figure 8. Air side (top) and fuel side (bottom) of the cells and interconnector of layer 1 (left) and layer 2 (right) during the stack disassembly.

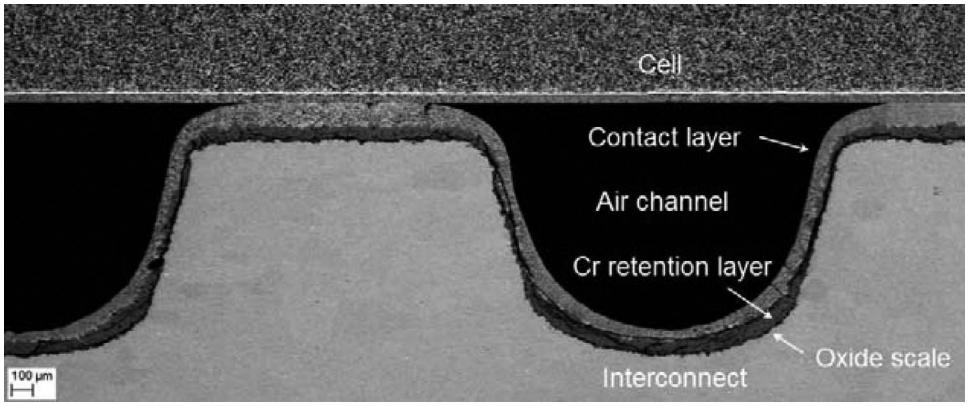

Figure 9. General morphology of the main stack components after operation.

of the cell. Furthermore, the combustion also led to severe oxidation and even the melting of a thin metallic sheet below the cell, which finally blocked the air channels. This also explains the large observed diffusion polarization in layer 2 at the last impedance measurement (Figure 4 and Figure 7). The thin metallic sheet worked as a glass holder for cell sealing on the air channels. In Figure 8, the thin sheets can be only seen in layer 1.

- All glass sealants for the cells and interconnectors were intact. No indication of leakages through the glass could be noticed. Indeed, the gas leakage test using a pressure drop method at room temperature after dismounting from the test bench indicated that the external gas tightness still fulfilled the quality requirement for new stacks. The rising of the stack temperature, starting from ∼18,000 h (Figure 1) and the corresponding decreasing of OCV of layer 2 (Figure 3) must be related to the burning process in layer 2. However, the decreasing of the OCVs in both cells already started at ∼8000 h, which contradicted the finding of the post-mortem analysis, that there were no leakages through glass and cells observed, especially in layer 1. It was later confirmed by maintenance of the test bench that there was a small hydrogen leak on the inlet side through the welding seam below the baseplate of the test bench. On the basis of the OCVs, the leakage rate of hydrogen was estimated to be less than 3% at the end of the testing period.

Detailed post-mortem analyses are ongoing. Changes in the microstructures and compositions of the cells, as well as the diffusion/transport of Ni, Mn, Sr and Cr, are of most importance, especially in comparison to SOFC operation. Interdiffusion among interconnector, glass and all other stack components shall be also investigated, and the results will be published subsequently. A preliminary analysis of the results will be given in this work. The cross section in Figure 9 shows the general situation of the main stack components after operation, recorded with back-scattered electrons (BSE). Except for the cracks inside the contact and Cr retention layers (but only in the region of the air channels, not on the contact ribs), all components were intact. The thin layer of Cr_2O_3 oxide scale below the Cr retention layer on the air side was about 5∼10 µm thick under higher magnification. On the fuel side, the thickness of the oxide scale was less than 5 µm. According to Megel et al.,[25] the growth of the oxide scale in the Crofer 22 APU with porous MCF coating could lead to a degradation rate of 0.4 mΩcm^2/1000 h at 850°C. Assuming a similar degradation rate with dense MCF coating at 800°C (as a very conservative assumption) and also taking into account the stack geometry, the maximal increase of the ASR due to oxide growth after 20,000 h of stack operation at 800°C would be less than 16 mΩ, which is less than 10% of the total increase in ohmic resistance (Figure 5).

The cross section of layer 2 on the fuel inlet side is shown in Figure 10. Due to the severe burning nearby, the electrolyte and air electrode on the contact ribs were destroyed. A strong interaction between the electrolyte, air electrode and contact coating took place. The exact reason for the leakage and fire in this region is still under intensive investigation. Preliminary results indicated that this would mostly be related to the imperfection in the air electrode of cell 2, where dozens of holes deep to the GDC barrier layer were observed near the burning location.

Beyond the burning location, both cells were in a comparable condition. Figure 11 shows the BSE images of both cells (air electrode at the bottom). The adhesions of all layers were intact inside the cells, especially the thin GDC layer prepared by physical vapor deposition (PVD). Some isolated pinholes could be found in the electrolyte, but there were no cracks throughout the electrolyte. The porosity of the region between the electrolyte and fuel electrode seemed higher than usual. Images with higher magnification showed that nearly half of the fuel electrode's functional layer near the outlet became much more porous after the long-term electrolysis operation. Figure 12 shows not only the magnified cross section of cell 1, but also a cross section of the same type of cell after ∼36,000 h of fuel cell operation at 700°C for comparison. Furthermore, the microstructure of the fuel electrode of cell 1 along the flow direction was compared, and is shown in Figure 13. In both positions (fuel inlet and outlet), there is the porous layer directly facing the electrolyte. In comparison, this layer is thicker at the fuel inlet than the fuel outlet position. Using energy-dispersive X-ray spectroscopy (EDX), no or relatively small amounts of nickel could be found at this part. Directly next to this very porous part, a dense layer could be found. To better quantify this phenomenon, 9–10 SEM images at three different locations were acquired and analyzed via ImageJ (porosity) and analySIS (thickness of the layers). The layers are marked by colored lines on the left side of the figure. These were adjusted at the bent forms of the layers. The former fuel electrode functional layer is marked in blue on the right

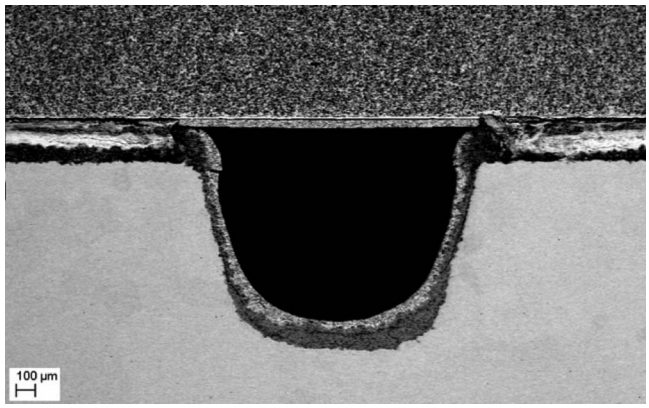

Figure 10. Cross section of layer 2 on the fuel inlet side.

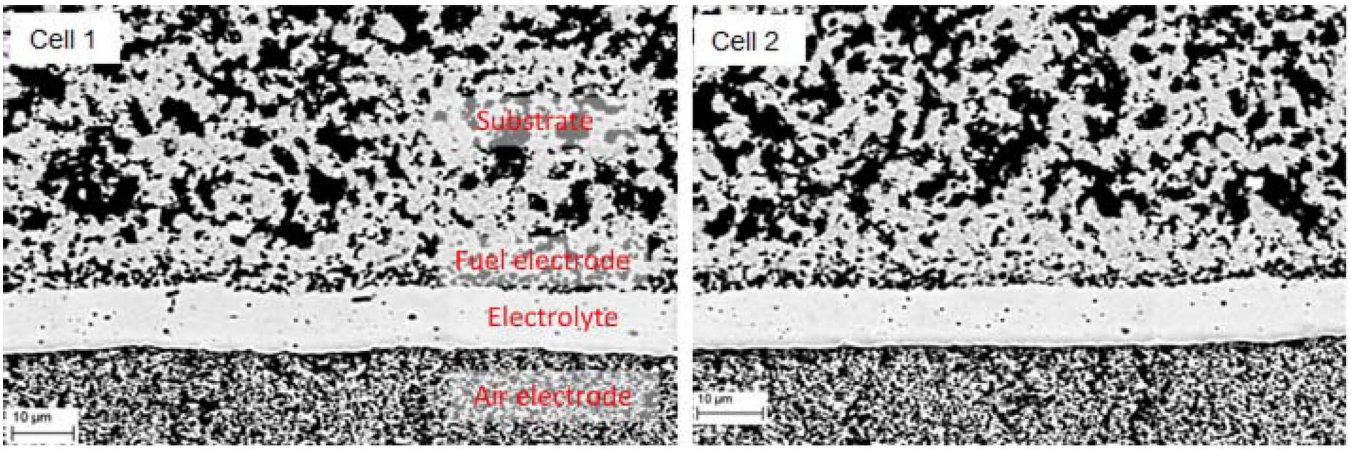

Figure 11. SEM cross sections of both cells near the fuel out let (without burning).

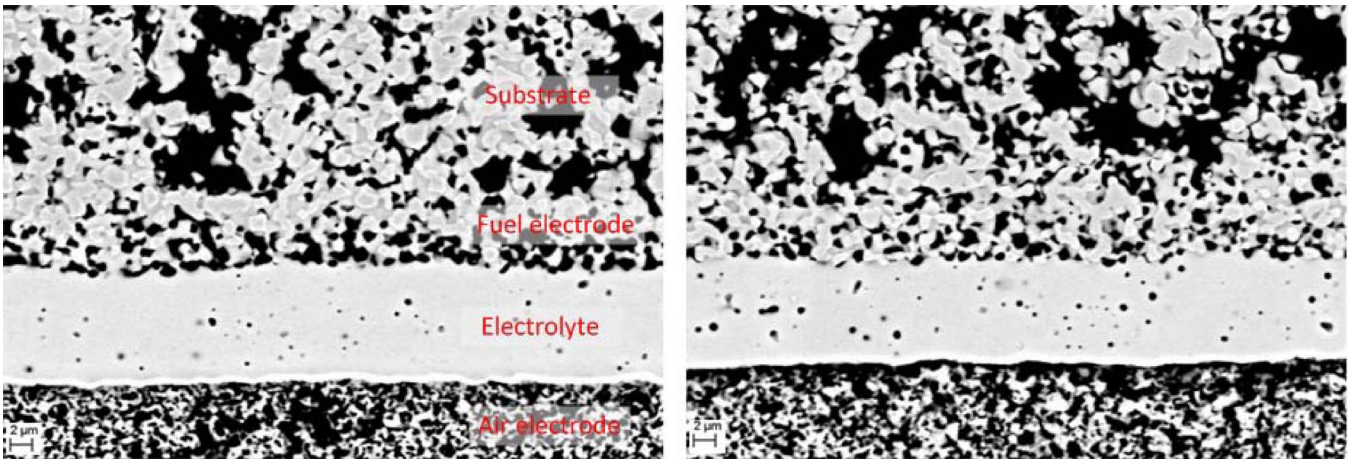

Figure 12. SEM cross sections of (left) cell 1, and (right) the same type of cell after ∼36,000 h of fuel cell operation at 700°C showing obvious difference in the porosity of the region at the electrolyte/fuel electrode interface.

side. The mean values and variance of the results are displayed in Table II and Table III.

The expected value for the porosity of the substrate is approximately 35%. The slightly larger porosity can be explained by the agglomeration of nickel, which also fits to the DRT analysis in Figure 6 and Figure 7, where the first peak corresponding to the gas diffusion in the substrate was decreasing with the operating time. However the porosity of the fuel electrode near the electrolyte is continuously rising from fuel outlet to inlet. With values between 36–45% all porosities are above the expected porosity of ∼20% for the pristine reduced fuel electrode. Similar phenomenon has been observed before and interpreted as the depletion of nickel.[19,26] The thickness of this layer

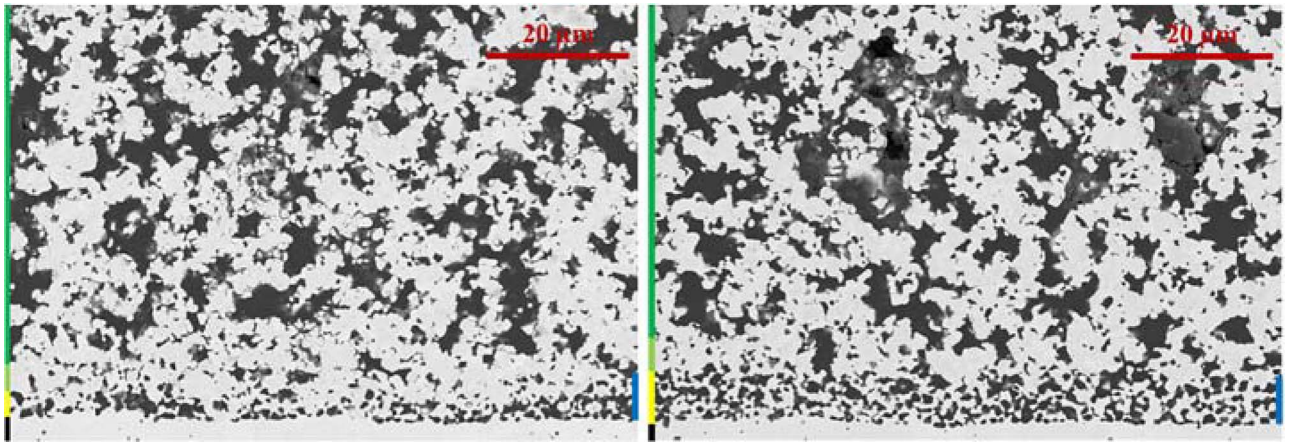

Figure 13. SEM cross sections of the fuel electrode of cell 1: (left) fuel outlet and (right) fuel inlet. Areas marked with colored lines: dark green: substrate, light green: dense layer, yellow: porous layer, black: electrolyte, blue: fuel electrode functional layer.

Table II. Porosity of the fuel electrode and substrate.

Location	Fuel outlet	Mid cell	Fuel inlet
Porous layer	36 ± 3%	42 ± 1%	45 ±2%
Dense layer	18 ± 2%	19 ± 1%	33 ± 3%
Substrate	38 ± 1%	38 ± 3%	39 ± 3%

Table III. Thickness of the porous layer.

Location	Fuel outlet	Mid cell	Fuel inlet
Thickness	3.0 ± 0.2 μm	3.7 ± 0.3 μm	6.7 ± 0.6 μm

is also increasing in the direction of the fuel inlet. In particular, at the fuel inlet the thickness of the layer is doubled. This might be explained with the composition of the gaseous atmosphere at the various locations inside the stack. Under electrolysis operation, there is a higher amount of steam and a relatively lower amount of hydrogen at the inlet compared to the outlet. Therefore the atmosphere at the inlet is more oxidizing in comparison to the outlet. Amongst others, the transportation of nickel is assumed to be conducted via nickel hydroxides and takes place especially at places with higher oxidation potential and steam concentration, e.g., at the fuel inlet.[26] The dense layer directly next to the porous region is the location at which the nickel seems to be condensed. This phenomenon leads to a shift in the triple-phase boundary and an enlargement of the porous electrolyte thickness, leading to higher ohmic resistance, as described previously. With a porosity of about 33% at the fuel inlet, this dense phase is not as pronounced. There are three possible explanations for this fact: 1) The nickel is more equally distributed in the neighboring substrate; 2) the nickel has been carried downstream with the fuel gas; 3) as reported in the literature, nickel simply depletes out of the cell. The slightly higher porosity of the substrate at the fuel inlet compared to other parts of the cell supports theory 2 or 3. However, all assumptions regarding the formation of nickel hydroxides must still be confirmed.

Conclusions

A Solid Oxide Cell (SOC) short stack consisting of two ASCs (anode in fuel cell mode) was assembled. Long-term electrolysis operations were carried out at 700°C, 750°C and 800°C under constant current mode with a current density of -0.5 Acm^{-2} and steam conversion rate of 50%, with 50% humidified H_2. A short fuel cell operation was also performed at 800°C for about 1500 h without noticeable degradation. During the first 8000 h of operation, there was almost no deterioration in the gas tightness of the stack/cells. The average ASR degradation rates at three temperatures were ∼10%/kh, despite a larger difference in the voltage degradation rates. Starting from 8000 h, the voltage and ASR degradation rates for the next 10,000 h of electrolysis at 800°C were ∼0.4%/kh and 2.7%/kh, respectively. After 10,000 h of endurance operation, the OCVs of the cells decreased from above 1.2 V to 1.1 V with dry H_2, which was later proven to be due to a leakage in the test bench (≤3%). The average degradation rates of the stack for the operation period of ∼18,460 h before the severe leakage in layer 2 started, including the losses during all load cycles and the intermediate fuel cell operation for 1500 h were 0.6%/kh and 8.2%/kh for the voltage and ASR degradation at 800°C, respectively. Impedance measurement and DRT analysis showed, and which was confirmed by post mortem analysis, that the main degradation mechanism was the continuously increased ohmic resistance, mainly due to a decrease in the effective conductivity of the fuel electrode as a result of Ni depletion in the electrode functional layer. Compared to the increase in the ohmic resistance, the degradation of the electrode polarization was virtually negligible. However, a continuous slight growth of polarization in the air electrode could be noticed throughout the stationary operation. Delamination of the air electrode was also observed in both layers after operation. Whether the slightly increased air electrode polarization was really related to the delamination is difficult to confirm, because the delamination of air electrode might be also caused by resin infiltration. Preliminary post mortem analysis revealed no process affecting the stack performance significantly, except for the Ni-depletion in the functional layer of the fuel electrode. Detailed analyses of the cells are ongoing, and the results will be published subsequently. During the last ∼2600 h of operation, the leakage rate was dramatically increased in layer 2, most likely as a consequence of the burning at the fuel inlet side. The exact reasons are not confirmed yet. One possible explanation was attributed to the imperfections in the cell, since many holes deep to GDC barrier layer were observed in layer 2, which was not the case in layer 1. However, this has to be furthermore examined in detail.

Acknowledgments

The cooperation with all colleagues working on SOC topics at the Forschungszentrum Jülich is greatly acknowledged. The authors thank in particular all colleagues in the department of FOB at the IEK-3 for maintaining the endurance test, Dr. Carole Babelot from the ZEA-1 for conducting the post-mortem analysis of the stack, Andreas Everwand from IEK-3 and Dr. Doris Sebold from IEK-1 for SEM operation.

ORCID

Qingping Fang https://orcid.org/0000-0002-2812-6866

References

1. J. Schefold, A. Brisse, and M. Zahid, *ECS Trans.*, **28**(11) 357 (2010).
2. Q. Fang, M. Heinrich, and C. Wunderlich, Crofer22 APU in Real SOFC Stacks, in *Advances in Solid Oxide Fuel Cells VII: Ceramic Engineering and Science Proceedings,* Volume **32** (eds N. P. Bansal, P. Singh, S. Widjaja, and D. Singh,), John Wiley & Sons, Inc., Hoboken, NJ, USA (2011).
3. A. Wood, H. He, T. Joia, and C. C. Brown, *ECS Trans.*, **66**(3) 23 (2015).
4. S. Megel, M. Kusnezoff, W. Beckert, N. Trofimenko, C. Dosch, A. Weder, M. Jahn, A. Michaelis, C. Bienert, M. Brandner, S. Skrabs, W. V. Schulmeyer, and L. S. Sigl, *CFY-Stacks: Progress in Development*, in In *Proceedings of 12th European SOFC and SOE Forum, A0908, European Fuel Cell Forum* (2016).
5. G. Rinaldi, S. Diethelm, E. Oveisi, P. Burdet, J. Van herle, D. Montinaro, Q. Fu, and A. Brisse, *Fuel Cells*, **17**, 541 (2017).
6. L. Blum, P. Batfalsky, Q. Fang, L. G. J. de Haart, J. Malzbender, N. Margaritis, N. H. Menzler, and Ro. Peters, *J. Electrochem. Soc.*, **162**(10), F1199 (2015).
7. L. Blum, U. Packbier, I. C. Vinke, and L. G. J. de Haart, *Fuel Cells*, **13**, 646 (2013).
8. N. H. Menzler, P. Batfalsky, S. M. Groß, V. Shemet, and F. Tietz, *ECS Trans.*, **35**(1), 195 (2011).
9. Q. Fang, L. Blum, P. Batfalsky, N. H. Menzler, U. Packbier, and D. Stolten, *Int. J. Hydrogen Energ.*, **38**, 16344 (2013).
10. L. Blum, Q. Fang, L. G. J. de Haart, J. Malzbender, N. Margaritis, N. H. Menzler, and Ro. Peters, *ECS Trans.*, **78**(1), 1791 (2017).
11. V. Nguyen, Q. Fang, U. Packbier, and L. Blum, *Int. J. Hydrogen Energ.*, **38**, 4281 (2013).
12. Q. Fang, L. Blum, and N. H. Menzler, *J. Electrochem. Soc.*, **162**(8), F907 (2015).
13. J. Szász, D. Klotz, N. H. Menzler, and E. Ivers-Tiffée, *Towards large-scale/industrial Fabrication of Anode-Supported Cells – Detailed Performance Study of Different Coating Techniques for Anode and Electrolyte*, In *Proceedings of 11th European SOFC and SOE Forum*, A1101, European Fuel Cell Forum (2014).
14. A. Leonide, V. Sonn, A. Weber, and E. Ivers-Tiffée, *ECS Trans.*, **7**(1) 521 (2007).
15. H. Geisler, A. Kromp, S. Hirn, A. Weber, and E. Ivers-Tiffée, *ECS Trans.*, **57**, 2691 (2013).
16. J. Weese, *Comput. Phys. Commun.*, **69**, 99 (1992).
17. J. Schefold, A. Brisse, and F. Tietz, *J. Electrochem. Soc.*, **159**, A137 (2012).
18. F. Tietz, D. Sebold, A. Brisse, and J. Schefold, *J. Power Sourc.*, **223**, 129 (2013).
19. D. The, S. Grieshammer, M. Schroeder, M. Martin, M. Al Daroukh, F. Tietz, J. Schefold, and A. Brisse, *J. Power Sourc.*, **275**, 901 (2015).
20. M. A. Laguna-Bercero, *J. Power Sourc.*, **203**, 4 (2012).
21. P. Moçoteguy and A. Brisse, *Int. J. Hydrogen Energ.*, **38**, 15887 (2013).
22. Y. Zheng, J. Wang, B. Yu, W. Zhang, J. Chen, J. Qiao, and J. Zhang, *Chemical Society Reviews.*, **5**, (2017).
23. Keqing Zheng and Meng Ni, *Sci. Bull.*, **61**(1), 78 (2016).
24. A. Leonide, *SOFC Modelling and Parameter Identification by Means of Impedance Spectroscopy*. Ph.D. thesis, Karlsruher Institut für Technologie (KIT), Karlsruhe (2010).
25. S. Megel, E. Girdauskaite, V. Sauchuk, M. Kusnezoff, and A. Michaelis, *J. Power Sourc.*, **196**, 7136 (2011).
26. M. B. Mogensen, A. Hauch, X. Sun, M. Chen, Y. Tao, S. D. Ebbesen, K. V. Hansen, and P. V. Hendriksen, *Fuel Cells*, **17**(4), 434 (2017).